Development of a slurry injection technique for continuous fibre ultra-high temperature ceramic matrix composites

Baker, Benjamin; Rubio Diaz, Virtudes ; Ramanujam, Prabhu; Binner, J.; Hussain, A; Ackerman, T.; Brown, P.; Dautremont, I.

DOI:
10.1016/j.jeurceramsoc.2019.05.070

Document Version
Peer reviewed version

Citation for published version (Harvard):
Baker, B, Rubio Diaz, V, Ramanujam, P, Binner, J, Hussain, A, Ackerman, T, Brown, P & Dautremont, I 2019, 'Development of a slurry injection technique for continuous fibre ultra-high temperature ceramic matrix composites', *Journal of the European Ceramic Society*, vol. 39, no. 14, pp. 3927-3937. https://doi.org/10.1016/j.jeurceramsoc.2019.05.070

Development of a slurry injection technique for continuous fibre ultra-high temperature ceramic matrix composites (UHTCMCs)

B. Baker, V. Rubio[a], P. Ramanujam[b], J. Binner, A. Hussain[c], T. Ackerman[c], P. Brown[d], I. Dautremont[e]

Affiliations

School of Metallurgy and Materials, University of Birmingham, Edgbaston, Birmingham, UK

a: Now with National Composites Centre, NCC, Bristol, UK

b: Now with Wendt India Ltd, Hosur, India

c: MBDA Missile Systems, Stevenage, UK

d: DSTL, Porton Down, UK

e: DGA, Paris, France

Abstract

A simple and effective slurry injection method for producing dense and uniform UHTCMCs from preforms of high fibre density was developed. As this method is based on slurry injection the homogeneity is not constrained to small preform sizes; dense components of high fibre volume can be produced in theoretically any size and shape. Samples produced by this method demonstrated high and consistent densities, with the injection method obtaining densities an average 27% higher and 87% lower in variability when compared to conventional vacuum impregnation. Tomography demonstrated no bias in the ceramic powder distribution for samples produced by injection, whereas samples produced by vacuum impregnation alone displayed poor powder penetration to the centre of large samples. The new approach yielded composites that were as strong and/or more consistent in strength compared to vacuum impregnation. Thermo-ablative testing demonstrated significant improvements with regards to protective capability for materials produced by this route.

Keywords:

Ceramic matrix composites, Slurry impregnation, CT analysis, Injection, Ultra-high temperature ceramics

1 Introduction

Vehicles for hypersonic regimes require well defined control surfaces with sharp leading edges in order to maximise manoeuvrability and aerodynamic efficiency, however the sharper the leading edge the more aggressive the resulting conditions, especially heat flux and therefore temperature, will be [1].

Maintaining both hypersonic velocities and high manoeuvrability thus requires leading edge components with high oxidation resistance and structural integrity. Temperatures of over 1900°C and associated stagnation point pressures of 150 MPa [2, 3] dictate the use of materials of high thermal conductivity, melting point, oxidation resistance and toughness [4]. Potential candidate materials for this application are ultra-high temperature ceramic matrix composites (UHTCMCs), materials that generally consist of a ceramic matrix and a woven reinforcement phase of carbon or silicon carbide fibres.

Ultra-high temperature ceramics, UHTCs, consist of a number of borides, carbides and nitrides of early transition metals, such as ZrB_2, HfB_2, HfC and TiC, whose melting points exceed 3000°C [5], exhibit high oxidation resistance, and retain structural performance at high thermomechanical loads [6]. An additional desire is for materials whose oxidation products provide some form of oxidation passivation for in-use components [7].

The incorporation of these ceramics into CMCs has been extensively studied in recent years and several procedures have become commonplace for their fabrication. Iteration of infiltration and pyrolysis of pre-ceramic precursors (PIP) can produce dense and homogeneous components [8-11], but often leads to micro-pores and cracks from volume contraction and gaseous bi-product evolution [12-14]. In-situ reaction with molten metals (RMI) with carbon/boron pre-matrices to form UHTC phases can, again, produce a dense matrix, but the molten reactive liquids often degrade fibre quality whilst residual metal in final components can limit the desired thermal and mechanical performance [15-18]. Infiltration and decomposition of precursor gases, chemical vapour infiltration (CVI), to produce ceramic phases within a reinforcement produces highly dense and consistent matrices [19], but commercial processes, carried out isothermally, typically take 2 – 3 months to achieve such densities and subsequently become highly expensive [20]. As a result, the cheap and low-temperature method of slurry infiltration is frequently used to attempt to obtain relatively high ceramic density specimens. This can be performed under many conditions: in the case of laminated 2D composites by slurry pasting and lay-up [7, 21, 22], or in the case of woven preforms by positive pressure infiltration or vacuum infiltration. Reinforcements of the latter

type, especially 2.5 or 3 dimensional preforms, are often found to be difficult to impregnate by these methods, with high-viscosity slurries failing to penetrate deeply into the porous fibre bodies [23].

A full analysis of impregnation techniques found in the literature is quite difficult given the broad ranges of slurry composition, viscosities, volatilities, wetting, reinforcement structure and conditions used; meaningful conclusions are hard to justify. In particular, there is a lack of data on many of these variables; numerous studies simply opt to describe the composite and omit important fabrication details. Nevertheless, common features across materials that are found to be hard to impregnate are primarily large preform sizes [24, 25] and 3D architectures [25, 26], whilst the use of large particle sizes in the slurry [25, 27] and volatile carrier fluids [27, 28] cause similar issues. Penetration mechanics resulting in the clogging effect [29] of larger particles observed at the entrance of micro porosity, as in fibre tows, means that these variables are very relevant. Likewise, high viscosity liquids will require larger timescales during pressure-assisted impregnation methods to achieve the same extent of penetration into a given substrate for a specific pressure gradient. Volatile fluids and high solid loading slurries are likely, therefore, to be problematic for a vacuum impregnation process. Sun et al [24] report a $ZrSiO_4$ modified C_f/C composite, with zircon powders being infiltrated *in vacuo* as an aqueous slurry. This material showed good penetration of powders up to 3 mm from the surface, but with ceramic content reducing as the distance increased. Jayaseelan et al [27] observed a similar penetration depth for ZrB_2 slurries based on ethanol. It was suggested that this was due to the exterior pores becoming clogged by powder, with the inner porosity thus becoming inaccessible. Other authors [30] suggest that residual inner macropores may be created by the increased viscosity of the slurries at higher solids content as a result of the evaporation of the often volatile solvents used as suspension carriers [31] in vacuum assisted processes.

Different authors have reported both good [32] and poor [25] infiltration into fibre bundles. Wu et al [32] described good bundle penetration as a result of small particle sizes and high levels of wetting of the slurry on the fibres, as it was a capillary pressure induced process. Work by Leslie et al [33] attempted to establish the conditions for optimal slurry impregnation in a SiC_f/HfB_2 system. They determined that, with a low solid content slurry, applied pressure provided superior loading than

vacuum methods and that with a vibration-assisted applied pressure route, the particle packing was enhanced. Subsequent work [34] showed that higher solid loadings resulted in a far lower extent of impregnation, however. In particular, the smaller channels in the preform were unfilled, suggesting that the increased viscosity of the higher solids content slurry had a negative impact on impregnation efficiency. Low solid content, however, translates into low UHTC powder content in the final composites, which can reduce oxidation resistance significantly. Similar results have been obtained by the current research team [28, 35, 36]. Slurries containing both UHTC powder and a carbon matrix precursor were used for the production of HfB_2 modified C_f/C test pieces. These slurries contained a high volume percentage of both UHTC powder and resin precursor. During the vacuum impregnation, the volatile acetone carrier phase would evaporate, leaving a highly viscous resin/powder mixture as the pore infiltrant, resulting in low impregnation consistency through-thickness for large components. Hence, an injection process was devised for the introduction of slurry into the main body of composite components, a process that has also been partially automated for the production of large test pieces. This paper describes the work underpinning this emerging process and the relative performances of materials produced through this process versus a vacuum only process in both thermoablative and mechanical testing.

2 Materials and methods

2.1 Slurry preparation

HfB_2 (70 wt% coarse powder, d_{50} 7.6 µm, H.C. Starck, Karlsruhe, Germany; 30 wt% fine powder, d_{50} 3.4 µm, Treibacher, Austria) slurries were produced in a fluid medium of phenolic resin (J2027L Cellobond, Momentive, UK) and acetone (AR grade, Sigma Aldritch, Dorset, UK) in a vol% ratio of 10.6 : 45.4 : 44 of HfB_2 : phenolic resin : acetone. ZrB_2 (d_{50} 3.1 µm, H.C. Starck, Karlsruhe, Germany) slurries were also produced in a fluid medium of phenolic resin and acetone (AR grade, Fischer Scientific, Loughborough), in a compositional spectrum using a solid loading of 20 vol% with the ratio of resin : acetone varying from 1 : 0 to 0.2 : 0.8. All slurries were ball milled for 48 h in polyurethane lined plastic bottles with alumina milling media. They were characterised using cone and plate (HfB_2) and parallel plate (ZrB_2) geometries on an AR500 Rheometer (TA Instruments, New Castle, USA).

2.2 Composite fabrication

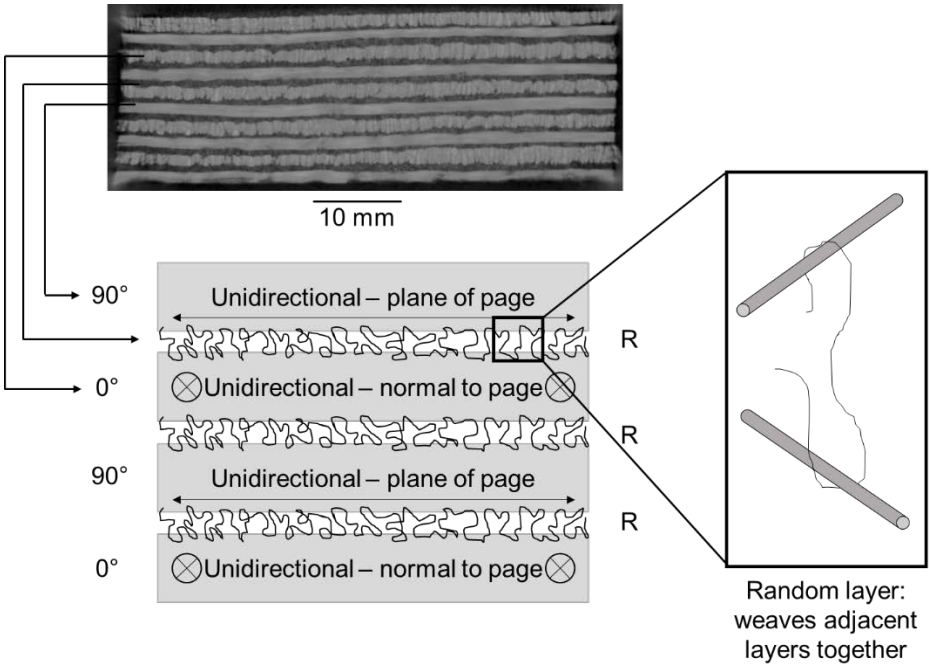

Figure 1: An X-ray tomogram showing the structure of the carbon fibre preforms and a schematic to illustrate how the constituent layers were formed and held together.

2.5D carbon fibre (C_f) preforms were sourced from Surface Transforms plc., Cheshire, UK. Fibre architecture was critical to the impregnation of the fibre preform materials. Figure 1 shows a micro-CT image of the preform structure. The material consisted of layers of unidirectional fibres organised into tows of 300,000 fibres of 10 µm diameter, stacked in orthogonal layers. These were defined as 0° and 90°, when in plane and out of plane respectively. The intervening spaces between these layers consisted of a lower density woven layer, joining adjacent unidirectional layers as indicated in the schematic in Figure 1. The structure of this layer was created by the manufacturer's needling process and is effectively random. The macro- and micro-scale details of the fabric are shown in Figure 2. The 2.5D nature is obtained by fibres that needle through perpendicular to the unidirectional layers from one randomly woven layer to the next, as shown in Figure 2c. Unlike 3D preforms, there is no through-thickness fibre reinforcement, but a degree of delamination resistance is obtained by the stitching of adjacent layers.

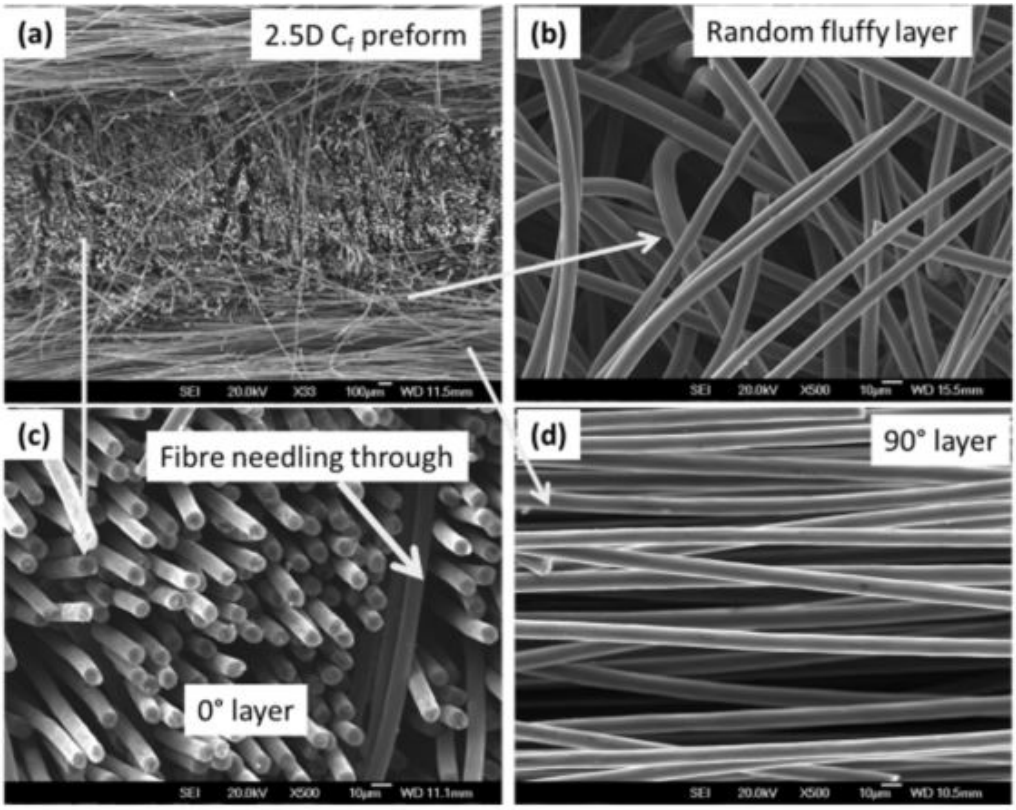

Figure 2: Scanning electron microscopy images of a cross-section of the carbon fibre preforms.

Two fabrication methods were compared, contrasted and combined in this work: the vacuum impregnation process (VI) and the injection assisted vacuum impregnation process (IVI).

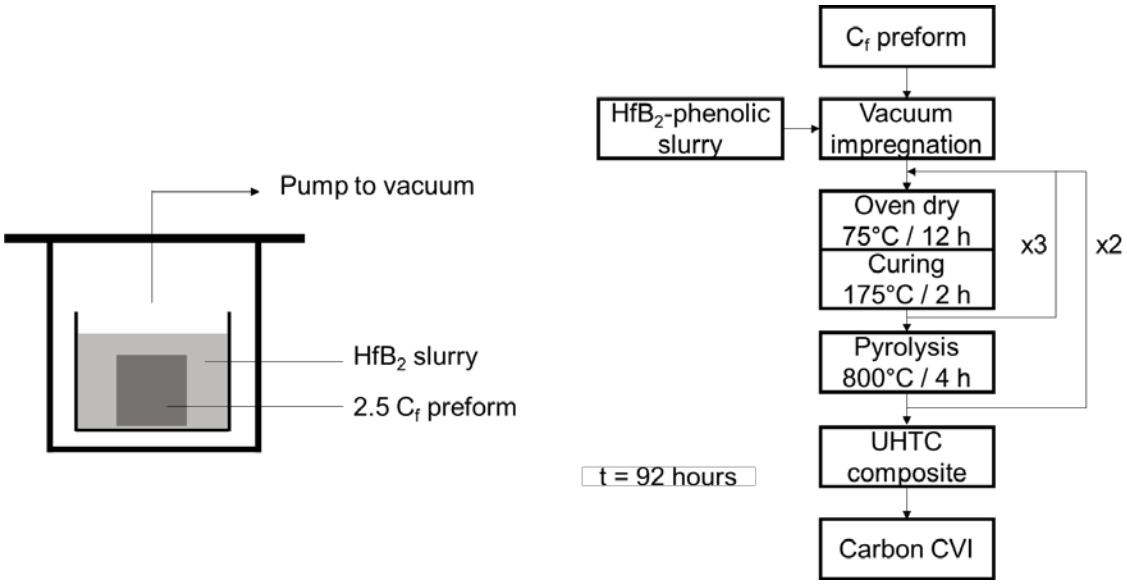

Figure 3: A schematic of the vacuum impregnation step and flow chart for the VI process.

The VI process consisted of submersion of the C_f preforms of the desired size in a bath of slurry within a vacuum chamber followed by pumping to a low pressure of 10^3 Pa. The amount of slurry required depended upon the size of the preform and size of the container; the preform needed to be submerged for the whole process. The slurry was forced into the woven preform by the negative pressure differential. This formed a thick surface layer of slurry and resin that needed to be carefully removed before being dried at 75°C and cured at 175°C to prevent vast reductions in perform permeability. This process was repeated twice before the composite was pyrolysed at 800°C for 4 hours under flowing argon. This entire process was repeated once more to produce the final component. This level of repetition was found to be required in order to maximise the amount of UHTC powder that was retained within the preform.

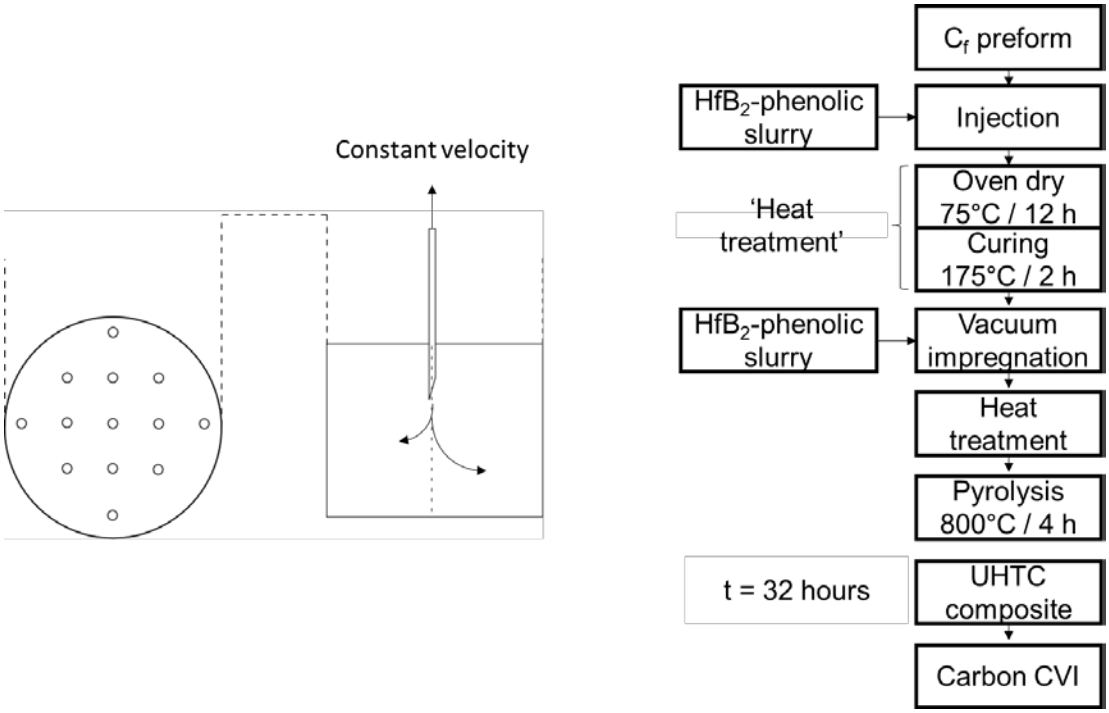

Figure 4: A schematic of the injection process and flow chart for the IVI process.

The IVI process consisted of injection of the slurry directly into the carbon fibre fabrics, as depicted in Figure 4. The needles used were 21 gauge, bevelled at an angle of 16°. Initial work focused on investigating the injection parameters so that the spread of the slurry within the preform material could be understood and optimised to allow dense and homogeneous components to be produced. Single

injections, rows and columns of injections at different spacing, and finally matrices of injections were produced and the results analysed, primarily using micro computed tomography. Early on, it was concluded that injecting the slurry smoothly into the preform as the needle was raised at a constant speed yielded superior results to making a series of individual deposits at different depths as the needle was withdrawn in a series of steps. Thus the 'smooth' approach was used during the subsequent work. The optimum speed for withdrawing the needle during injection was found to be ~4.5 mm s^{-1} for the fibre preforms being used, with a slurry flow rate of approximately 0.25 cm^3 s^{-1}. For larger samples intended as test components, the injections were made across the whole of the sample in a grid of injection points with the best nearest-neighbour spacing determined to be 5 mm and using an outwards spiral injection pattern, injecting first the centre of the preform then moving progressively outwards to the edges. For the investigation of injection mechanics, an automated injection system was developed. A schematic of the system is shown in Figure 5 and it consisted of a CNC router fitted with a syringe and needle, connected to a magnetically agitated slurry tank via a peristaltic pump. Pressure was applied to the syringe via a compressor and an automatic dispenser module. This set-up permitted quantification of injection pressure and slurry feed rate. The main utility of the automated process in this investigation was in the reproducibility of the injection conditions. The CNC and automatic dispenser were programmed to deliver slurry evenly over the course of an injection, the ejection rate of slurry matching the withdraw rate of the needle tip. A slurry injection rate of approximately 0.08 cm^3 s^{-1} was used, and two applied pressures of 0.2 and 0.3 MPa were investigated. The needle was connected to the barrel of the syringe via a double Luer lock. This was found to partially mitigate the relatively common issue of settling of the ceramic suspension. The needle occasionally became clogged with particulates and the double Luer lock prevented the pressure blowing the needle tip off the syringe.

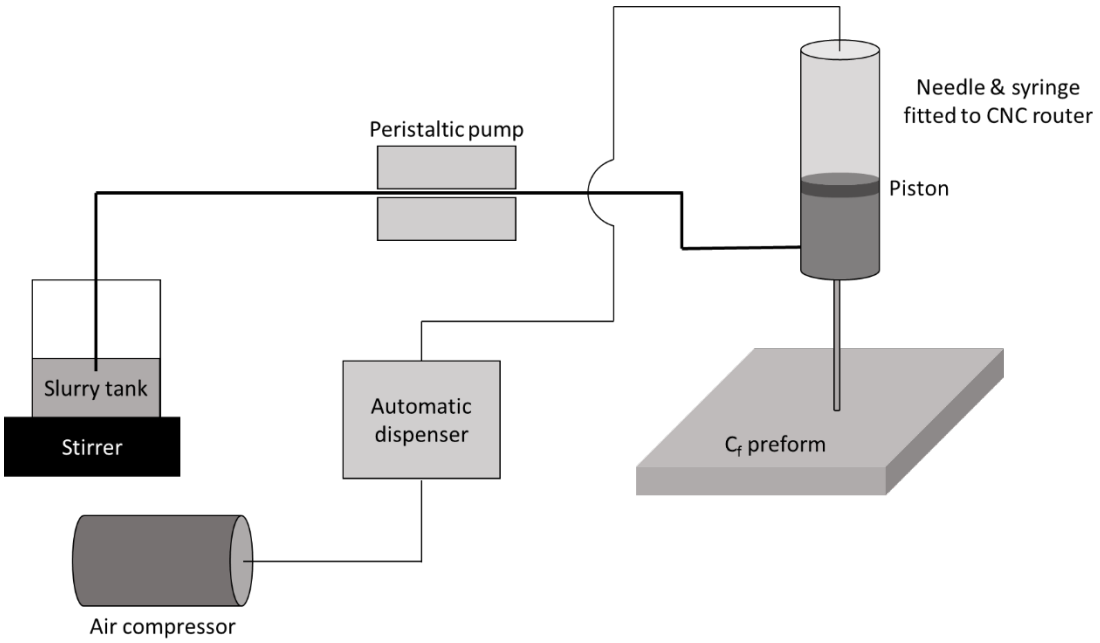

Figure 5: A schematic of the automated injection process.

Following injection, the samples were dried in an oven at 75°C and cured at 175°C. Since it was observed that the injection process was not very good at filling the preform right up to the edges, the samples were subsequently given a single vacuum impregnation step, dried and cured again using the same conditions and then pyrolysed at 800°C for 4 hours under flowing argon. Thus in the injection vacuum impregnation, IVI, process each step was undertaken only once. In the results section, all material densities presented have been calculated geometrically.

As indicated earlier, the spreading behaviour of the slurry in the carbon fibre preforms was primarily analysed using X-ray micro-CT at an accelerating voltage of 200 kV and current of 150 µA. Composites were also analysed using optical microscopy, SEM and EDX (Jeol 6060 SEM with Oxford Inca EDX, Peabody, USA) to determine powder penetration efficacy. Image analysis was performed using ImageJ software (Java-based image processor, National Institutes of Health and the Laboratory for Optical and Computational Instrumentation, Bethesda MD, US) and binary images were produced using colour thresholding. This consisted of assigning a colour intensity value to each pixel and producing a false-colour image where each pixel above a certain intensity was displayed as white whilst those below were black.

2.3 Performance testing

The strength of the IVI-processed composites was measured and compared to that of the VI-processed materials. Details of the measurement procedures may be found elsewhere [37]. Oxyacetylene torch testing proceeded in a purpose built facility at the University of Birmingham, as described in previous publications [28]. Flow rates of 0.8 m^3 $hour^{-1}$ for acetylene and 1.1 m^3 $hour^{-1}$ were used, obtaining testing temperatures of approximately 2900°C. The samples were fixed in a water-cooled graphite sample holder, and rotated directly into the flame to begin the test. The front face temperature was measured by both a 2-colour pyrometer and an infrared camera. The rear face temperature was measured with a k-type thermocouple. Samples were analysed by laser confocal microscopy (KEYENCE, Itasca IL, USA) to analyse surface topography.

3 Results and Discussion

3.1 Fabrication and route development

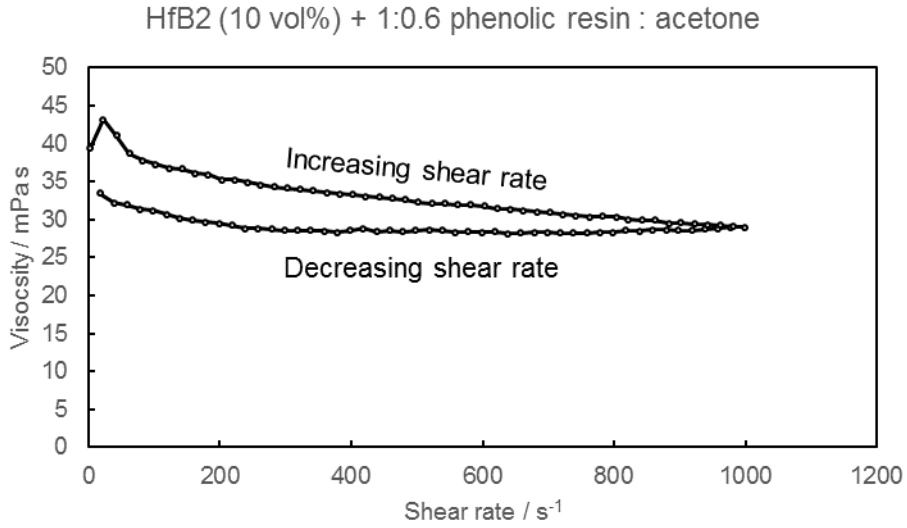

Figure 6: The shear dependant viscosity of the HfB_2 slurries for the analysis of the injection process.

The shear-dependant viscosities of the HfB_2/phenolic resin/acetone slurry are shown in Figure 6. It was found to be shear-thinning, with a viscosity of 31 mPa s at 117 s^{-1}. This value of strain rate was chosen as

an arbitrary comparator for the slurries produced and is not representative of the strain rate over the course of an injection. Figure 7 shows the steady-state viscosity of the ZrB_2 slurries used to investigate the effect of slurry viscosity on the deposit morphology. It can be seen that the viscosity increased exponentially with phenolic resin content as expected.

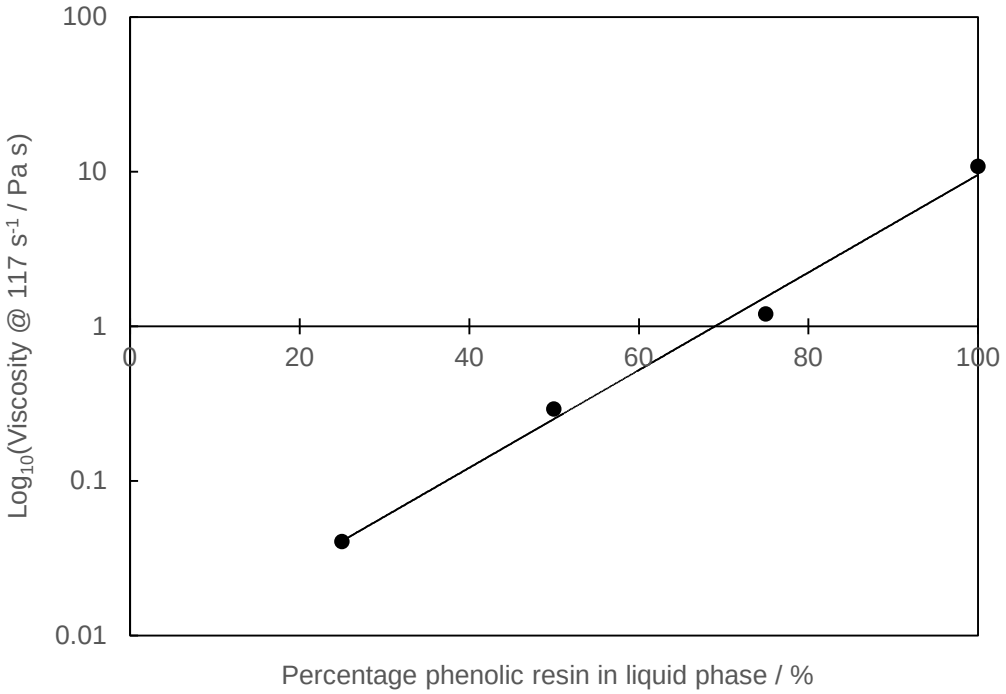

Figure 7: The viscosity, at a shear rate of 117 s^{-1}, of a series of ZrB_2 : phenolic resin : acetone slurries, at a solid content of 20 vol%.

Samples made through the VI process were observed to have an inhomogeneous ceramic distribution, as shown in the X-ray tomogram in Figure 8.

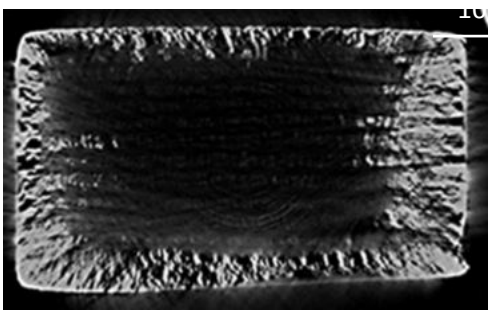

Figure 8: X-ray CT image of a C_f/C-HfB_2 sample produced by the VI approach; the brighter regions contained more HfB_2 powder.

The deposition was concentrated almost exclusively at the surface of the preform, penetrating to a maximum of 7 mm into the centre. Whilst this would provide initial thermal and oxidation protection, if the impregnated layer were damaged or overmatched, then rapid component oxidation and, potentially, failure could follow. In addition, the mechanical strength would be compromised from the start. Worse; any component produced by this method will require final machining to shape and this will inevitably result in the removal of most of the surface layer of the component even before use. The poor penetration efficiency was thought to be due to the slurry finding difficulty in being drawn deeply into the preform channels through capillarity by the pressure gradient obtained by the vacuum. The enhanced viscosity due to drying of the high vapour pressure acetone resulted in high solids content resin phases becoming immobile in channels, clogging the preform close to the surface and preventing further impregnation. Other work by this group performed through aqueous processing routes using a low viscosity, low volatility 20 vol% ZrB_2 slurry demonstrated the presence of powder to a depth of over 15 mm at a concentration of greater than 20%. The solution to this clogging problem, whilst desiring to retain the high solids content, and hence viscous slurry, and volatile resin/acetone system was seen to be the development of an injection-based process.

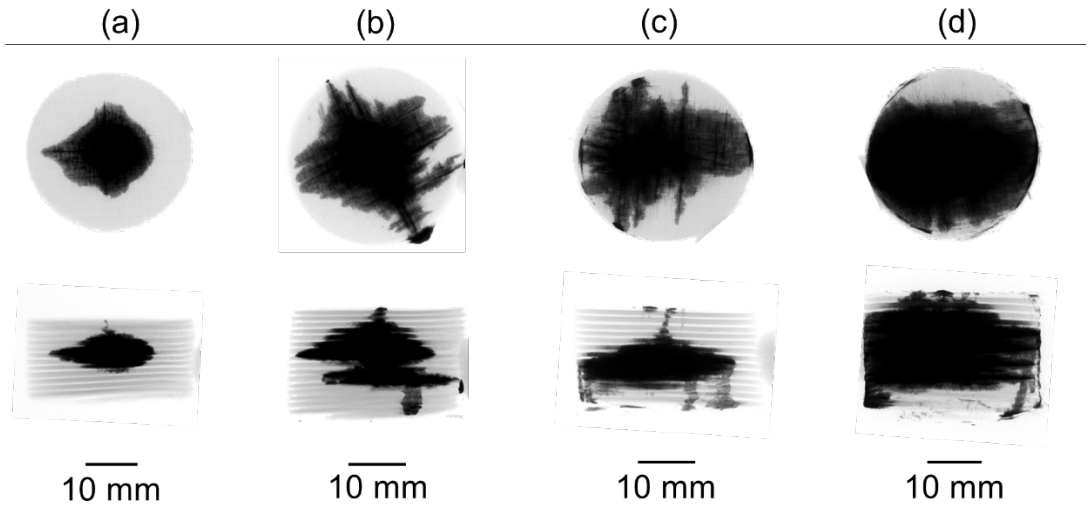

Figure 9: X-ray tomograms of 1 cm^3 injections of slurry, (a) a single injection, (b) a vertical column of three injections spaced by 5 mm apart, (c) a horizontal line of injection points spaced 5 mm apart, (d) a 3x3 vertical grid of injection points spaced 5 mm apart.

Figure 9a shows the ceramic distribution resulting from a single injection of ~1 cm^3 of slurry; the result was a rough ellipsoid of ~1.6 cm^3. This corresponds to a porosity of around 15 vol%, indicating good filling of the fibre layers. No significant gradient in ceramic density is visible close to the injection point. For three injections spaced 5 mm apart vertically, Figure 9b, it can be seen that the merging of the slurry was not homogeneous. This was probably due to the layered structure of the fibre preform, with differences in local density and anisotropic permeability. In contrast, and as expected, three injections the same distance apart horizontally, Figure 9c, yielded a pattern with large in-layer spreading, but little between the adjacent layers. When nine injections were created in a two-dimensional matrix, Figure 9d, the result was a reasonably homogeneous spread, lacking significant voids between the injection points. The fibrous architecture was relatively unperturbed by this process; the deposit fills the porosity and only small channels may be seen in the structure, as indicated in Figure 10a.

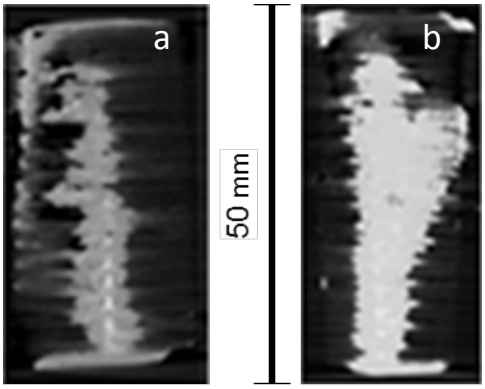

Figure 10: X-ray computed tomograms showing the spreading resulting from columnar injections. (a) as a series of individual deposits at different depths as the needle was withdrawn in a series of steps and (b) by injecting it as the needle was raised smoothly at a constant velocity of ~4.5 mm s^{-1}.

Figure 10 shows the results from injecting the slurry as a series of individual deposits at different depths as the needle was withdrawn in a series of steps and by injecting it as the needle was raised smoothly at a constant speed of ~4.5 mm s^{-1}. It can be seen that the latter approach yielded a much more homogeneous columnar deposit and hence was used in all future experimentation.

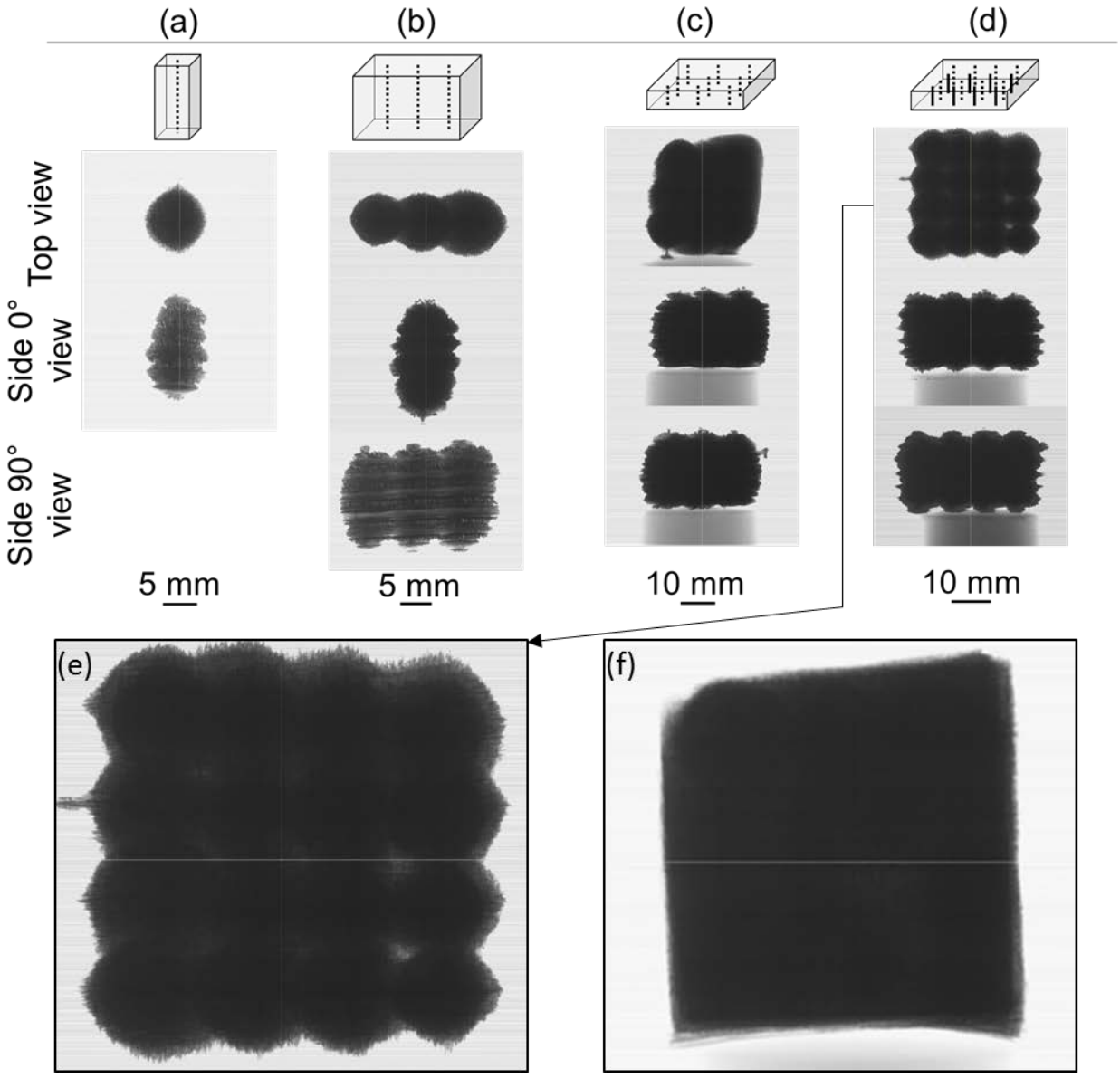

Figure 11: X-ray computed tomograms showing the spreading resulting from columnar injections. (a) a single column, (b) three parallel columns, (c) a 3x3 matrix of columns, (d) a 4x4 matrix of columns and (e) and (f) enlarged views of the 4x4 matrix sample made using piston pressures of 0.2 and 0.3 MPa respectively. All injection spacings were 5 mm apart.

Figure 11 shows the spreading resulting from columnar injections using the smooth injection approach into the preforms. Figure 11a shows that a cylindrical column of HfB_2 powder deposit was created, which was axisymmetric and had an apparent volume of 3.14 cm^3. As shown in Figure 11b & c, the slurry merged homogeneously without obvious porosity when first one row of 3 columns and then a matrix of

three rows of three columns were created. If Figure 11b is considered more closely, however, it may be seen that the radii of the columns increase from left to right. This fits with the chronological order in which the injections were made, i.e. when a second column is injected next to the first the already deposited slurry perturbs the spatial distribution on one side, preventing the column being axisymmetric. This effect is also present in the 3x3 grid, with later injections deviating outwards more as the injections proceeded anti-clockwise in the image. It can just be seen in Figure 11d that in the case of a 4x4 grid produced using the automated injection system, low solids loading regions were present in the diagonal spaces between injections. A larger image of the same result is provided in Figure 11e for clarity. In an attempt to improve the homogeneity of the powder deposit, the piston pressure applied was increased from 0.2 to 0.3 MPa. The result may be seen in Figure 11f and given the success observed, the higher pressure was used for all further sample preparation.

From the Hagen-Poiseuille equation for flow through a tube, equation (1), it can be seen that both the applied pressure differential and the fluid viscosity impact the flow rate of the liquid, and hence the expected flow through the preform, proportionally and inversely respectively:

$$Q = \frac{\Delta P \pi R^4}{8 \mu L} \tag{1}$$

where: Q is volumetric flow rate ($m^3\ s^{-1}$), ΔP is the pressure difference between ends of the tube (Pa), R is the radius of the tube (m), μ is the dynamic viscosity of the liquid (Pa s) and L is the length of the tube (m). This explains why the use of a higher piston pressure led to the improved spreading seen in Figure 11f compared to Figure 11e.

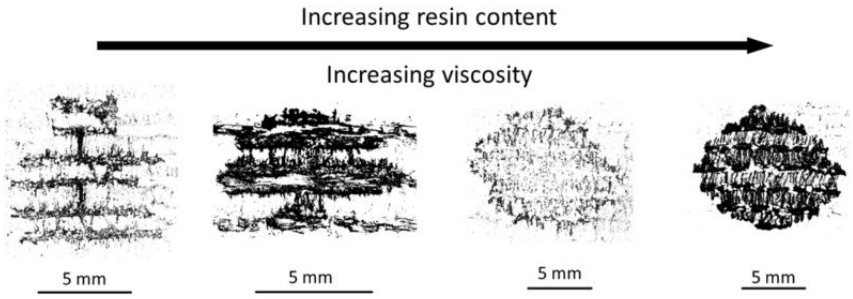

Figure 12: Optical microscopy images showing the characteristic morphologies of ceramic powder deposits formed by single injections of the four different viscosity slurries shown in Figure 7.

The effect of the slurry viscosity on the deposit morphology was also investigated. It can be seen in Figure 12 that increased viscosity slurries yielded a more compact and circular impregnation morphology. As the viscosity was increased, a transition occurred from preferential filling of the lower density randomly woven layers to more homogeneous filling of all the layers. This is an important consideration when judging material consistency and hence the protective capability for these composites. If the highest concentration of UHTC material only exists within the randomly woven layers, this is unlikely to provide adequate oxidation resistance for the fibres most responsible for the structural properties, viz., the unidirectional tows. Also, the porosity structure seen in the two left-hand most images in Figure 12 is unlikely to be conducive to achieving a high thermal conductivity perpendicular to the fabric layers; a key material selection criterion for UHTCMCs.

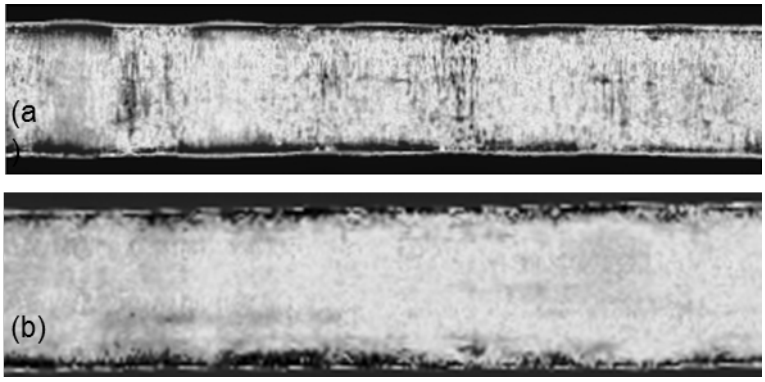

Figure 13: X-ray computed tomograms showing the effect of injection spacing on the ability to impregnate the carbon fibre preforms homogeneously; (a) 10 mm spacing, (b) 5 mm spacing.

The consequences of using the IVI approach to impregnate the carbon fibre preforms may be seen in Figure 13. Both impregnations used the optimum process conditions, but in (a) the spacing of the injections were 10 mm apart, whilst in (b) they were 5 mm apart. It may be seen that the latter yielded the more homogeneous filling of the preform demonstrating why this became the standard for use in later work. Comparison of Figure 13a & b shows how consistent the impregnation of the powder was throughout the whole of the preform when the optimised IVI process was used.

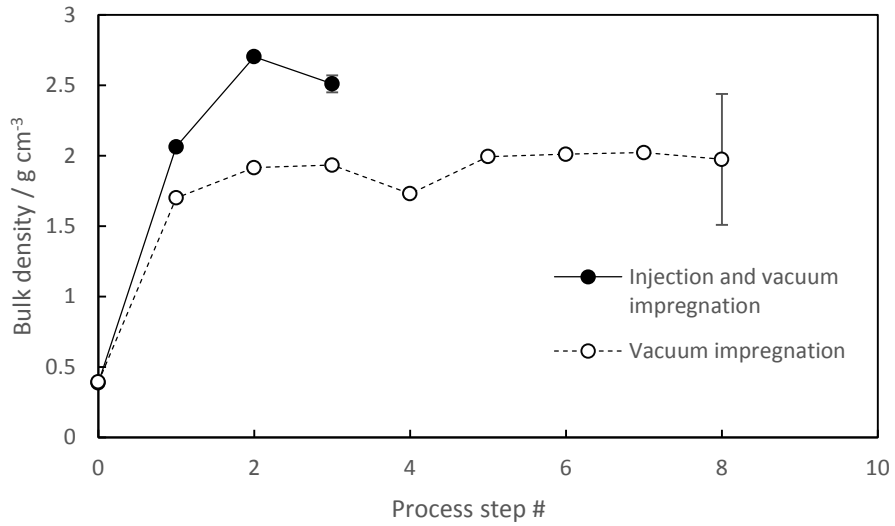

Figure 14: Comparison of the density evolution for samples made via the injection & vacuum impregnation route (IVI) to vacuum impregnation (VI) only as a function of the process steps described in Figure 3 and Figure 4. The variability in final component density is indicated.

In addition, it can be seen from Figure 14 that, for equally sized samples, the production of higher density pieces was obtained by the first process step of IVI, in addition to substantially higher and more consistent final densities; 2.51 ± 0.06 g cm^{-3} compared to 1.96 ± 0.47 g cm^{-3}. This compares to the theoretical density (assuming the porosity is filled by a slurry medium of ratio 10.6 : 45.4 HfB_2 : phenolic resin) of 4.89 g cm^{-3}. The five fewer process steps represent 60 hours less spent on producing samples of superior density and this also came at the benefit of reduced material costs. For large samples, the automated system also provided a means of infiltrating preforms without the need for the many manual injections required for full impregnation. This resulted in high efficiency work.

Two equations were derived that would model the quantity of slurry needed for the IVI and VI processes as shown below:

Injection $$V_{slurry} = \frac{v_{cf} V_{preform}}{E_I} \quad (2)$$

$$= \frac{\pi h_p (1 - v_{cf}) {r_p}^2}{E_I}$$

Vacuum impregnation

$$V_{slurry} = \frac{A_{container} h_{sample}}{E_{VI}} = \frac{\pi h_p (r_p + \delta r)^2}{E_{VI}} \quad (3)$$

where the required slurry volume (V_{slurry}) for a single impregnation process is presented as a function of fibre volume fraction (v_{cf}), preform volume ($V_{preform}$, cylindrical with radius r_p), container cross sectional area ($A_{container}$, cylindrical with radius $r_p + \delta r$), sample depth (h_p) and impregnation efficiency (E_x). The latter is an expression of the degree of porosity left after impregnation, such that a value of $E_x = 1$ would represent zero residual porosity, i.e. a completely efficient impregnation procedure.

It can immediately be seen that for $E_I = E_{VI}$, the quantity of slurry will be much greater for the VI process as the volume required is that of the slurry bath up to at least the height of the preform rather than simply the preform volume. However, $E_I \neq E_{VI}$ since, as this work has shown, the centre of the sample remains unimpregnated with the VI approach, Figure 15. In addition, the proportion of the volume of this ceramic-rich shell to the whole preform volume will decrease as the volume increases, leading to an apparent sizable reduction in E_{VI} as the preform size increases. This simple analysis indicates the wastefulness inherent to the VI process. In addition, recycling of the slurry is not trivial with the VI process since the slurry contains a high volume fraction of volatile carrier solvent and is kept at low pressure during the process, leading to a large amount of evaporation. This adds significant procedural complications due to the associated change in viscosity and solid loading, which will reduce the reproducibility of impregnation cycles unless significant quality assurance testing and corrections to the composition are made during the fabrication of composite samples. In general, therefore, it is easier to simply make fresh slurry for each sample processed by VI, although with costly powders this can quickly become uneconomical. The injection process, in contrast, does not suffer from these limitations since only as much slurry as is needed to fill each preform's porosity is used and hence there is no need to try

to recycle the slurry. A single VI step at the end of the process ensures that the surface layers have a high ceramic concentration, important for both flexural strength and ablation resistance.

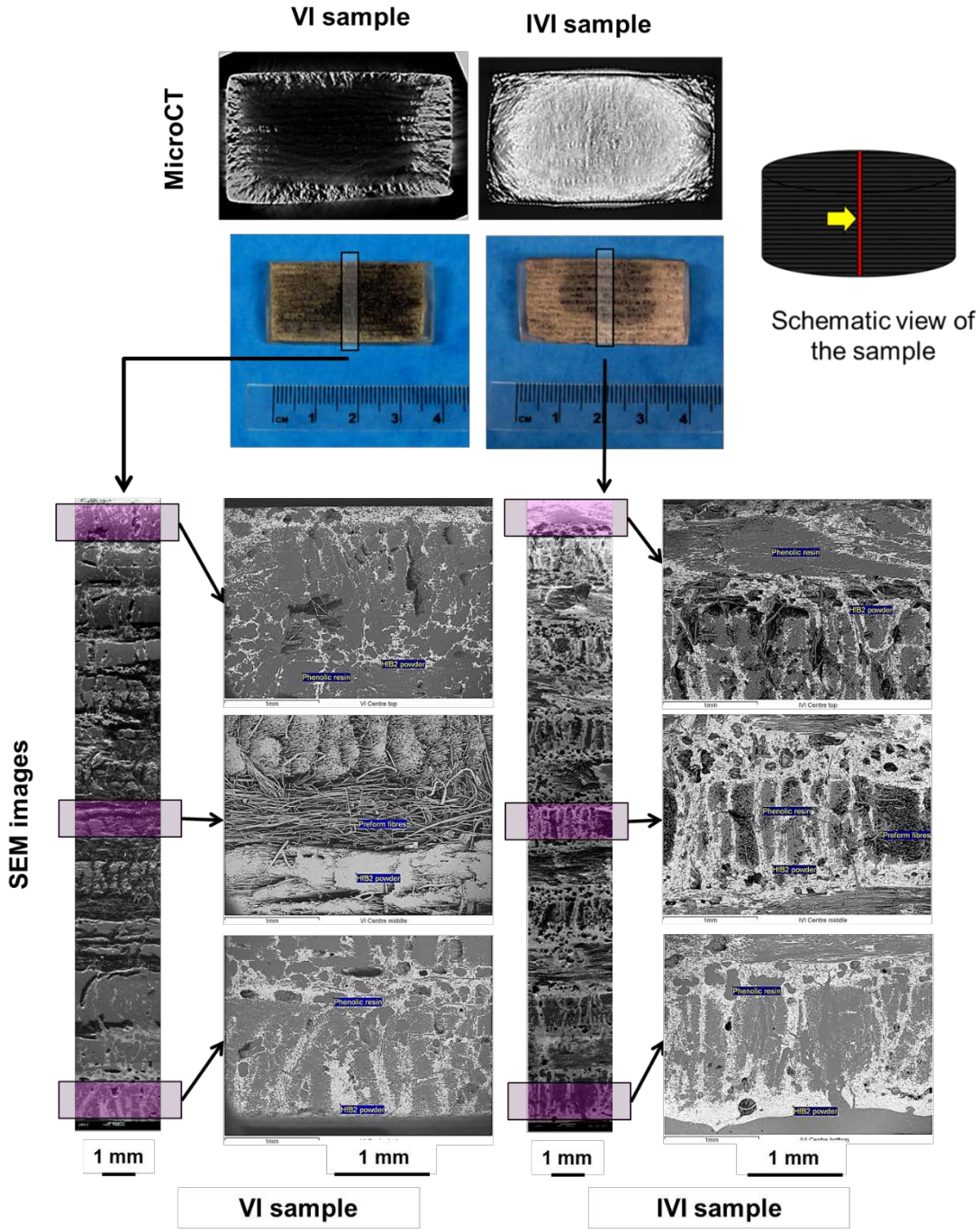

Figure 15: Microstructural and tomographic characterisation of samples produced by the IVI route compared to the VI route.

Figure 15 shows a collage of images from two similar sized samples made by the VI and IVI processes. It reinforces the result that penetration of the powder into the centre of the composite does not occur with the VI process if the sample size exceeds twice the penetration depth of the slurry into the preform (typically 4 – 7 mm). Note that the discolouration on the photograph of the IVI sample is unfortunately due to cutting and does not indicate a large porous space. The micro-CT image indicates good ceramic distribution throughout the preform.

3.2 Performance testing of samples produced through VI and IVI

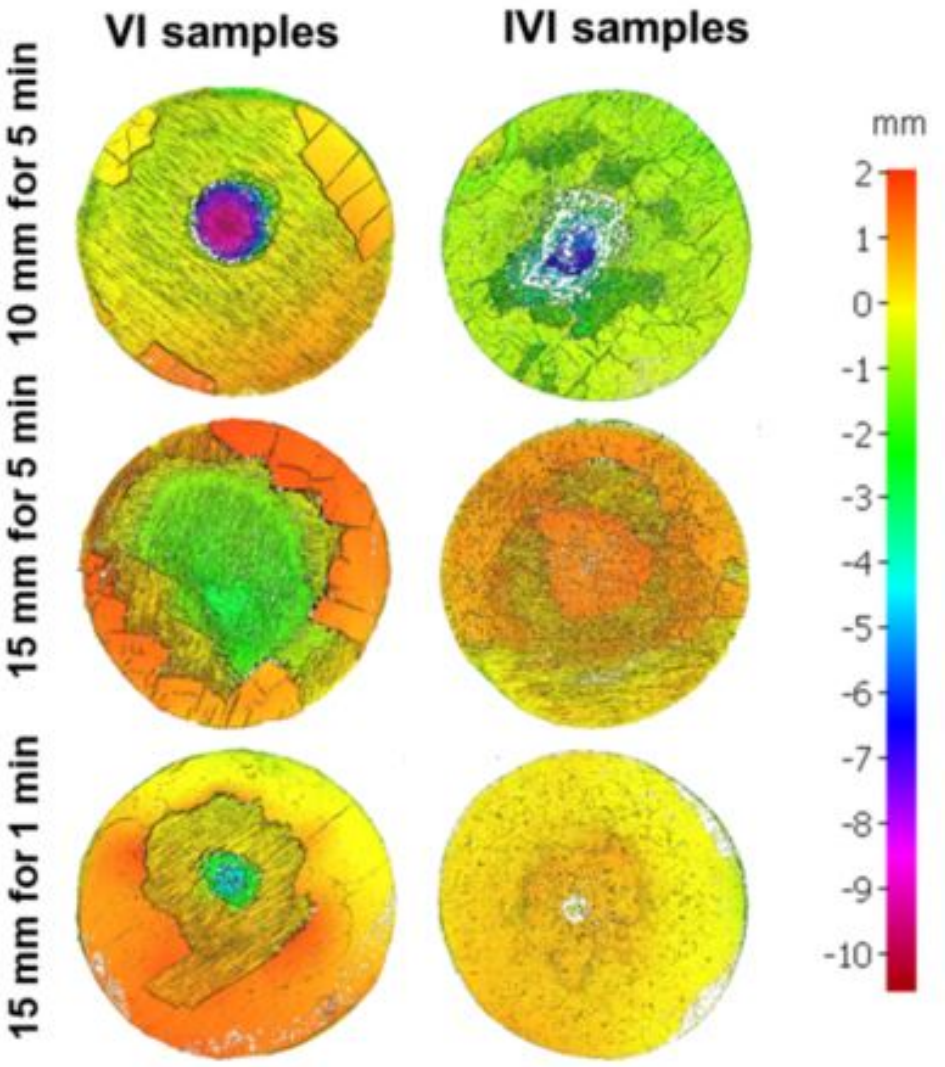

Figure 16: Confocal microscopy images of samples produced through the VI and IVI processes respectively, after OAT testing using 2 different distances between the nozzle and the sample and 2

different times (shorter distances and longer times are more destructive). The colour scale indicates the surface profile of the sample after ablation; yellow is calibrated to the original sample surface height.

Figure 16 shows the ablated surfaces of samples tested by oxy-acetylene torch testing, at around 2900°C. For the samples tested for 1 minute with 15 mm between the nozzle and sample surface, it can be seen that the IVI sample demonstrated no denudation, rather there was production of a thin oxide layer on the surface. The VI sample, however, demonstrated a clear crater of up to 5 mm in depth. Increasing the time to 5 minutes resulted, in the case of the IVI sample, in an increase in the oxide layer's thickness and consistency over the whole surface. The VI sample in contrast shows a very large hole in the surface, where a substantial volume has been destroyed by the flame. Decreasing the distance, and consequently significantly increasing the incident heat flux and gas velocity to 17 MW m^{-2} and 206 m s^{-1} respectively, resulted in far greater ablation for both samples. However, whilst the IVI sample showed a hole reaching 5 – 6 mm in depth and fairly consistent material ablation across the rest of the face, the VI sample had a deep crater bored into the surface reaching over 10 mm in depth. This illustrates perfectly the effect of reduced ceramic loading within the centre of the composite; once the surface layer was breached, the oxidation and combustion of the centre progressed rapidly and a wide hole was formed (it should be noted that the diameter of the actual flame was approximately 3 mm).

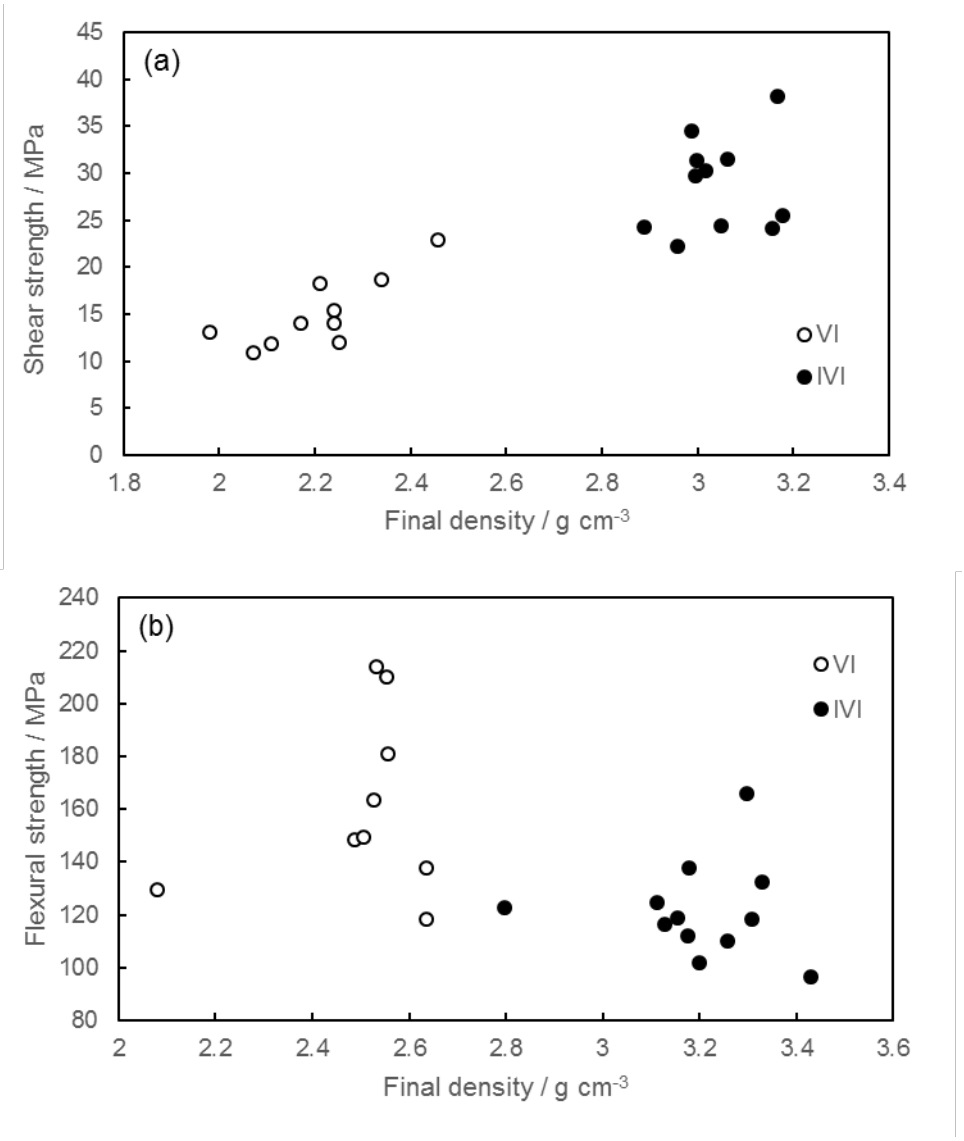

Figure 17: (a) Shear and (b) flexural strength of samples produced by the IVI and VI routes, densified with pyrolytic carbon through isothermal CVI as a function of density.

Figure 17a shows the shear strength of samples produced via both methods with final densification achieved through the use of carbon deposited via CVI by Surface Transforms Ltd in the UK [37]. Samples produced through the IVI method demonstrate higher average final densities and shear strength, 3.04 ± 0.09 g cm^{-3} and 28.8 ± 5.0 MPa respectively, compared to 2.21 ± 0.13 g cm^{-3} and 15.1 ± 3.8 MPa for the VI samples. Clearly, the higher concentration of HfB_2 and its homogenous distribution within the preform results in a higher strength by approximately a factor of two. This contrasts with the flexural strength, where, although there is greater consistency in the values, a drop in strength is observed for

samples produced by the IVI method, an average of 121 ± 18 MPa compared to 161 ± 34 MPa for samples produced via VI alone. This difference is not statistically significant.

4 Conclusion

An injection vacuum impregnation method for the production of UHTCMCs has been successfully developed, negating the problems seen in some slurry systems surrounding ceramic homogeneity. X-ray micro-CT imaging suggests that powder distribution is far more consistent with respect to penetration depth than bulk infiltration via vacuum impregnation alone. IVI is useful for impregnating preforms of high fibre density that do not possess connected channels that will allow easy slurry ingress. In combination with the use of high solid-loading slurries of high viscosity, it also yields excellent powder homogeneity and permits impregnation where bulk methods like pressure assisted or vacuum assisted impregnation may fail. In addition, it is up to three times faster and suffers from little or no slurry wastage. Materials produced through an IVI route performed better, both in shear testing and thermoablatively, to comparable materials produced through the VI route. This is thought to be due to a higher concentration of ceramic powder within the centre of the preform, acting both as a strengthening feature and thermally conductive medium. While this study did not utilise fibre substrates with coatings, recent work [38] has found that a 500 nm pyrolytic carbon coating did not prevent substrates being injectable with ceramic slurries. Hence, this method may show promise in a variety of material systems with or without interface treatments.

Potentially, however, the greatest advantage of the process has not even been mentioned in this publication so far. Unlike other bulk infiltration techniques, the injection technique reported here can also be harnessed to produce heterogeneously dispersed composites, with different matrix phases sharing the same woven reinforcement, by the simple expedient of injecting different slurries in different locations. This is expected to overcome the structural issues often associated with lamination of different phases [39] in multi-layered materials. Work on this opportunity is currently well advanced and will be reported in the near future.

The IVI process demonstrates viability with regards to both superior component density and highly reduced total processing time. While this is attenuated by the increased person-hours as a proportion of total processing time, development of an automated system presented in this work has shown promise in decreasing this time and vastly improving sample reproducibility, suggesting that this method has scope for scale up and industrialisation.

Acknowledgements

The authors would like to acknowledge the funding from the *Ultra-High Temperature Ceramics Composite Materials*, MCM ITP programme, contract number UKG 7023, MBDA UK Ltd, 2014 – 2016 and also the *Processing Of UHTC Composites For Hypersonic Applications* programme, contract number DSTLX-1000085783, funded by DSTL, 2014 – 2016.

Conflict of interest

There are no conflicts of interest to declare.

References

[1] Marschall J, Fletcher DG. High-enthalpy test environments, flow modeling and in situ diagnostics for characterizing ultra-high temperature ceramics. Journal of the European Ceramic Society. 2010;30(11):2323-36.
[2] Savino R, Fumo MDS, Paterna D, Serpico M. Aerothermodynamic study of UHTC-based thermal protection systems. Aerospace Science and Technology. 2005;9:151-60.
[3] Savino R, Criscuolo L, Di Martino GD, Mungiguerra S. Aero-thermo-chemical characterization of ultra-high-temperature ceramics for aerospace applications. Journal of the European Ceramic Society. 2018;38(8):2937-53.
[4] Van Wie DM, Drewry DG, King DE, Hudson CM. The hypersonic environment: Required operating conditions and design challenges. Journal of Materials Science. 2004;39(19):5915-24.
[5] Tang S, Hu C. Design, Preparation and Properties of Carbon Fiber Reinforced Ultra-High Temperature Ceramic Composites for Aerospace Applications: A Review. Journal of Materials Science & Technology. 2017;33(2):117-30.
[6] Fahrenholtz WG, Hilmas GE. Ultra-high temperature ceramics: Materials for extreme environments. Scripta Materialia. 2017;129:94-9.
[7] Li L, Wang Y, Cheng L, Zhang L. Preparation and properties of 2D C/SiC–ZrB2–TaC composites. Ceramics International. 2011;37(3):891-6.
[8] Patra N, Al Nasiri N, Jayaseelan DD, Lee WE. Thermal properties of Cf/HfC and Cf/HfC-SiC composites prepared by precursor infiltration and pyrolysis. Journal of the European Ceramic Society. 2018;38(5):2297-303.

[9] Xie Z, Zhou T, Gou Y. Synthesis and characterization of zirconium diboride ceramic precursor. Ceramics International. 2015;41(5, Part A):6226-31.
[10] Zhang M-y, Li K-z, Shi X-h, Tan W-l. Effects of SiC interphase on the mechanical and ablation properties of C/C-ZrC-ZrB2-SiC composites prepared by precursor infiltration and pyrolysis. Materials & Design. 2017;122:322-9.
[11] He J, Gao Y, Wang Y, Fang J, An L. Synthesis of ZrB2-SiC nanocomposite powder via polymeric precursor route. Ceramics International. 2017;43(1, Part B):1602-7.
[12] Zhuang L, Fu Q-G, Liu T-Y. Ablation resistance of wedge-shaped C/C-ZrB2-ZrC-SiC composites exposed to an oxyacetylene torch. Corrosion Science. 2016;112:462-70.
[13] Ziegler G, Richter I, Suttor D. Fiber-reinforced composites with polymer-derived matrix: processing, matrix formation and properties. Composites Part A: Applied Science and Manufacturing. 1999;30(4):411-7.
[14] Yan C, Liu R, Zhang C, Cao Y, Long X. Mechanical behaviour and microstructure of Cf/ZrC, Cf/SiC and Cf/ZrC – SiC composites. Advances in Applied Ceramics. 2016;115(7):391-5.
[15] Wang D, Dong S, Zhou H, Kan Y, Wang Z, Zhu G, et al. Effect of pyrolytic carbon interface on the properties of 3D C/ZrC–SiC composites fabricated by reactive melt infiltration. Ceramics International. 2016;42(8):10272-8.
[16] Xiaowu C, Qian F, Le G, Xiangyu Z, Shaoming D, Jingxiao W, et al. Interphase degradation of three-dimensional Cf/SiC–ZrC–ZrB2 composites fabricated via reactive melt infiltration. Journal of the American Ceramic Society. 2017;100(10):4816-26.
[17] Zhang L, Dong S, Zhou H, Kan Y, Zhou F, Wang Z. 3D Cf/ZrC–SiC composites fabricated with ZrC nanoparticles and ZrSi2 alloy. Ceramics International. 2014;40(8, Part A):11795-801.
[18] Liu Y, Fu Q, Zhang J, Li L, Zhuang L. Erosion resistance of C/C-SiC-ZrB2 composites exposed to oxyacetylene torch. Journal of the European Ceramic Society. 2016;36(15):3815-21.
[19] Berthon S, Malé G. Infiltration of zirconium diboride by ICVI in porous materials. Composites Science and Technology. 1997;57(2):217-27.
[20] Golecki I. Rapid vapor-phase densification of refractory composites. Materials Science and Engineering: R: Reports. 1997;20(2):37-124.
[21] Uhlmann F, Wilhelmi C, Schmidt-Wimmer S, Beyer S, Badini C, Padovano E. Preparation and characterization of ZrB2 and TaC containing Cf/SiC composites via Polymer-Infiltration-Pyrolysis process. Journal of the European Ceramic Society. 2017;37(5):1955-60.
[22] Zoli L, Sciti D. Efficacy of a ZrB2–SiC matrix in protecting C fibres from oxidation in novel UHTCMC materials. Materials & Design. 2017;113:207-13.
[23] Tang S, Deng J, Liu W, Yang K. Mechanical and ablation properties of 2D-carbon/carbon composites pre-infiltrated with a SiC filler. Carbon. 2006;44(14):2877-82.
[24] Sun C, Li H, Fu Q, Zhang J. Microstructure and ablation properties of carbon/carbon composites modified by ZrSiO4. Corrosion Science. 2014;79:100-7.
[25] Li Q, Dong S, Wang Z, Hu J, Wu B, Zhou H, et al. Fabrication of a ZrC–SiC matrix for ceramic matrix composites via in-situ reaction and its application. Ceramics International. 2013;39(1):877-81.
[26] Wang D, Dong S, Zhou H, Zhang X, Ding Y, Zhu G. Fabrication and microstructure of 3D Cf /ZrC-SiC composites: through RMI method with ZrO2 powders as pore-making agent. Ceramics International. 2016;42(6):6720-7.
[27] Jayaseelan DD, de Sá RG, Brown P, Lee WE. Reactive infiltration processing (RIP) of ultra high temperature ceramics (UHTC) into porous C/C composite tubes. Journal of the European Ceramic Society. 2011;31(3):361-8.
[28] Paul A, Rubio V, Binner JGP, Vaidhyanathan B, Heaton ACJ, Brown P. Evaluation of the high temperature performance of HfB2 UHTC particulate filled Cf/C composites. International Journal of Applied Ceramic Technology. 2017;14(3):344-53.

[29] Feng Q, Wang Z, Zhou HJ, He P, Gao L, Kan YM, et al. Microstructure analysis of Cf/SiC–ZrC composites in both fabrication and plasma wind tunnel testing processes. Ceramics International. 2014;40(1, Part A):1199-204.
[30] Zhou H, Ni D, He P, Yang J, Hu J, Dong S. Ablation behavior of C/C-ZrC and C/SiC-ZrC composites fabricated by a joint process of slurry impregnation and chemical vapor infiltration. Ceramics International. 2018;44(5):4777-82.
[31] Smallwood IM. Handbook of Organic Solvent Properties2012.
[32] Wu B, Dong S, Wang Z, Kan Y, Zhang L, Zhou F. Properties of Cf/SiC composites modified by a boron- containing phase. Ceramics International. 2013;39(4):4729-34.
[33] Leslie C, Boakye E, Keller K, Cinibulk M. Development of Continuous SiC Fiber Reinforced HfB2-SiC Composites for Aerospace Applications. Processing and Properties of Advanced Ceramics and Composites V2013.
[34] Leslie C, Boakye E, Keller K, Cinibulk M. Development and Characterization of Continuous SiC Fiber-Reinforced HfB2-Based UHTC Matrix Composites Using Polymer Impregnation and Slurry Infiltration Techniques. International Journal of Applied Ceramic Technology. 2015;12(1):235-44.
[35] Paul A, Binner JGP, Vaidhyanathan B, Heaton ACJ, Brown PM. Heat flux mapping of oxyacetylene flames and their use to characterise Cf-HfB2 composites. Advances in Applied Ceramics. 2016;115(3):158-65.
[36] Paul A, Binner JGP, Vaidhyanathan B. UHTC Composites for Hypersonic Applications. In: Fahrenholtz WG, Wuchina EJ, Lee WE, Zhou Y, editors. Ultra-High Temperature Ceramics2014.
[37] Rubio V, Binner J, Cousinet S, Le Page G, Ackerman T, Hussain A, et al. Materials characterisation and mechanical properties of Cf-UHTC powder composites. Journal of the European Ceramic Society. 2019;39(4):813-24.
[38] Cheng Y, Hu P, Zhang W, Ma C, Feng J, Fan Q, et al. One-step introduction of ZrC-SiC inside carbon fabric to fabricate high homogeneous and damage-tolerant composite inspired by vibration. Journal of the European Ceramic Society. 2019;39(7):2251-6.
[39] Jayaseelan DD, Xin Y, Vandeperre L, Brown P, Lee WE. Development of multi-layered thermal protection system (TPS) for aerospace applications. Composites Part B: Engineering. 2015;79:392-405.